Peroxosolvates of Purine Derivatives: Structural Insights into H_2O_2-Purine Possible interactions in biological systems

Andrei V. Churakov,[a] Alexey A. Mikhaylov,[a] Elena A. Mel'nik,[a] Pavel A. Egorov,[a] Ovadia Lev,[b] Alexander G. Medvedev,[a] Petr V. Prikhodchenko,[a]*

Kurnakov Institute of General and Inorganic Chemistry, Russian Academy of Sciences, Leninskii prosp. 31, 119991 Moscow, Russia. E-mail: medvedev.chem@gmail.com

The Casali Center of Applied Chemistry, The Institute of Chemistry, The Hebrew University of Jerusalem, 9190401 Jerusalem, Israel

Experimental

X-ray crystallography

The samples were withdrawn from the crystallization vials using corrosion-resistant steel spatula and immediately placed inside a drop of perfluorinated Fomblin YR-1800 oil on the microscope slides. The appropriate single crystals were mounted on the top of Mitegen MicroLoops and transferred instantly to a cold nitrogen stream on the diffractometer.

Experimental data sets were collected on a Bruker SMART APEX II diffractometer (for **1**, **2** and **4**) and Bruker D8 Venture machine (for **3 and 5)** using graphite monochromatized Mo-*K*α radiation (λ = 0.71073 Å). All probed crystals of **3** exhibited non-merohedral twinning. The problem was resolved during integration procedure (APEX3 software).[4] Absorption corrections based on measurements of equivalent reflections were applied.[5] The structures were solved by direct methods and refined by full matrix least-squares on F^2 with anisotropic thermal parameters for all non-hydrogen atoms.[6] All hydrogen atoms were found from difference Fourier synthesis and refined with isotropic thermal parameters (except for disordered atoms H5B and H6B in **5**). In the structure **5**, hydrogen peroxide atom O5 is disordered over two positions with occupancy ratio 0.82(2)/0.18(2). H-atoms of minor component of disorder were placed on the lines connecting hydrogen bonded oxygen atoms at distances 0.85 Å from O_{peroxo} positions and they were refined using a riding model (AFIX 3) with $U_{iso}(H_{peroxo})=1.5\times U_{eq}(O_{peroxo})$. In all structures, the partial substitutional disorder of hydrogen peroxide by water molecules[7–10] was not observed since no residual peaks with an intensity more than 0.22 e/A^3 were seen around the centres of O-O bonds. The single-crystal X-ray diffraction studies were performed at the Centre of Shared Equipment of IGIC RAS. Crystallographic data deposited with Cambridge Structural Database (see Table 2 for details).

Elemental analysis. The hydrogen peroxide content in peroxosolvates was determined by iodometric titration. Carbon, hydrogen and nitrogen content were determined using the vario MICRO cube analyzer (Elementar, Germany).

X-ray powder diffraction measurements were performed on a D8 Advance diffractometer (Bruker AXS, Karlsruhe, Germany) with a goniometer radius of 280 mm. The powder samples were filled into low background quartz sample holders. XRD patterns in the range 5˚ to 60˚ 2θ were recorded at room temperature using CuKα radiation (λ=1.5418 Å) under the following measurement conditions: tube voltage of 40 kV, tube current of 40 mA, step scan mode with a step size 0.02˚ 2θ. XRD patterns were processed by DiffracPlus software.

Differential thermal analysis (DTA) and **thermogravimetry analysis** (TGA) were performed on simultaneous thermal analyzer, DTG-60 (Shimadzu). All experiments were carried out under argon flow at a heating rate of 10 °C/min.

FTIR spectra were recorded on a JASCO FT/IR-4600 spectrometer.

Solid-state DFT calculations.
The space groups and unit cell parameters of **1**, **3,** refcodes THEOPH08[11] and ZETPAT[12] obtained in the single-crystal X-ray studies are fixed and structural relaxations are limited to the positional parameters of atoms. Density functional theory computations with periodic boundary conditions (solid-state DFT) were performed in the Crystal23 software package[13] using B3LYP functional and the localized basis set 6-31G**. The mixing coefficient of Hartree-Fock/Kohn-Sham matrices is set to 25%. Tolerance on energy controlling the self-consistent field convergence for geometry optimizations and frequencies computations is set to 10^{-10} and 10^{-11} Hartree, respectively. The shrinking factor of the reciprocal space net is set to 3. The optimized structures are found to correspond to the minimum point on the potential energy surface.

The Bader analysis of the periodic electron density was performed using Topond21.[14]
The energy of intermolecular H-bonds E_{HB} is evaluated according to ref. [15] as:

$$E_{HB} = 1126 \cdot G_b \quad \text{(S1)}$$

where G_b is the positively-defined local electronic kinetic energy density at the H···O bond critical point.[16] The Espinosa approach gives reasonable results for energies of intermolecular H-bonds and other non-covalent interactions in organic crystals varying from 2.0 to 50 kJ mol^{-1}.[17]

Table S1. Crystal data and details of X-ray analysis.

	1 Theophylline $C_7H_8N_4O_2 \cdot H_2O_2$	**2 Theobromine** $C_7H_8N_4O_2 \cdot H_2O_2$	**3 Hypoxanthine** $2(C_5H_4N_4O) \cdot H_2O_2$	**4 Hypoxanthine** $2(C_5H_4N_4O) \cdot 3(H_2O_2)$	**5 Benzylaminopurine** $C_{12}H_{11}N_5 \cdot 2(H_2O_2)$
Empirical formula	$C_7H_{10}N_4O_4$	$C_7H_{10}N_4O_4$	$C_{10}H_{10}N_8O_4$	$C_{10}H_{14}N_8O_8$	$C_{12}H_{15}N_5O_4$
*F*w	214.19	214.19	306.26	374.29	293.29
colour, habit	colourless, prism	colourless, prism	colourless, plate	colourless, prism	colourless, needle
cryst size (mm)	0.50×0.50×0.20	0.40×0.40×0.35	0.10×0.08×0.01	0.30×0.20×0.20	0.25×0.04×0.04
tempreture (K)	150	100	100	100	100
crystal system	monoclinic	orthorhombic	triclinic	triclinic	monoclinic
space group	$P2_1/c$	*P*bca	*P*-1	*P*-1	$P2_1/c$
a (Å)	5.8540(1)	13.6261(3)	6.2828(4)	7.2682(3)	20.1096(8)
b (Å)	16.7182(4)	7.1632(1)	7.0513(4)	7.4476(3)	6.5746(3)
c (Å)	9.2006(2)	18.3896(3)	14.9231(8)	15.3478(6)	20.4108(8)
α (deg)	90	90	85.761(2)	89.808(2)	90
β (deg)	101.1707(8)	90	88.382(2)	77.703(2)	102.0852(14)
γ (deg)	90	90	65.266(2)	65.6040(10)	90
V (Å^3)	883.39(3)	1794.94(6)	598.83(6)	735.90(5)	2638.76(19)
Z	4	8	2	2	8
D_c (g·cm^{-3})	1.610	1.585	1.699	1.689	1.477
μ (mm^{-1})	0.134	0.132	0.136	0.147	0.114
F(000)	448	896	316	388	1232
θ range (deg)	3.55 to 30.00	3.40 to 28.99	1.37 to 28.99	3.14 to 26.99	2.04 to 27.00
refl collcd	10415	19915	3163*	8756	33180
indep reflns / R_{int}	2551 / 0.0188	2366 / 0.0234	3163* / 0.0559	3197 / 0.0196	5754 / 0.0441
reflns $I>2\sigma(I)$	2332	2210	2205	2784	4771
No of param	176	176	239	291	503
GooF on F^2	1.071	1.074	1.112	1.055	1.109
R_1 ($I>2\sigma(I)$)	0.0390	0.0355	0.0581	0.0382	0.0481
wR_2(all data)	0.1113	0.0961	0.1562	0.1010	0.1148
largest diff peak / hole (e·Å^{-3})	0.477 / -0.230	0.481 / -0.219	0.386 / -0.319	0.480 / -0.240	0.289 / -0.316
CCDC number	2455936	2455938	2468621	2455939	2455937

* TWINABS (Bruker, 2012) absorption correction used.

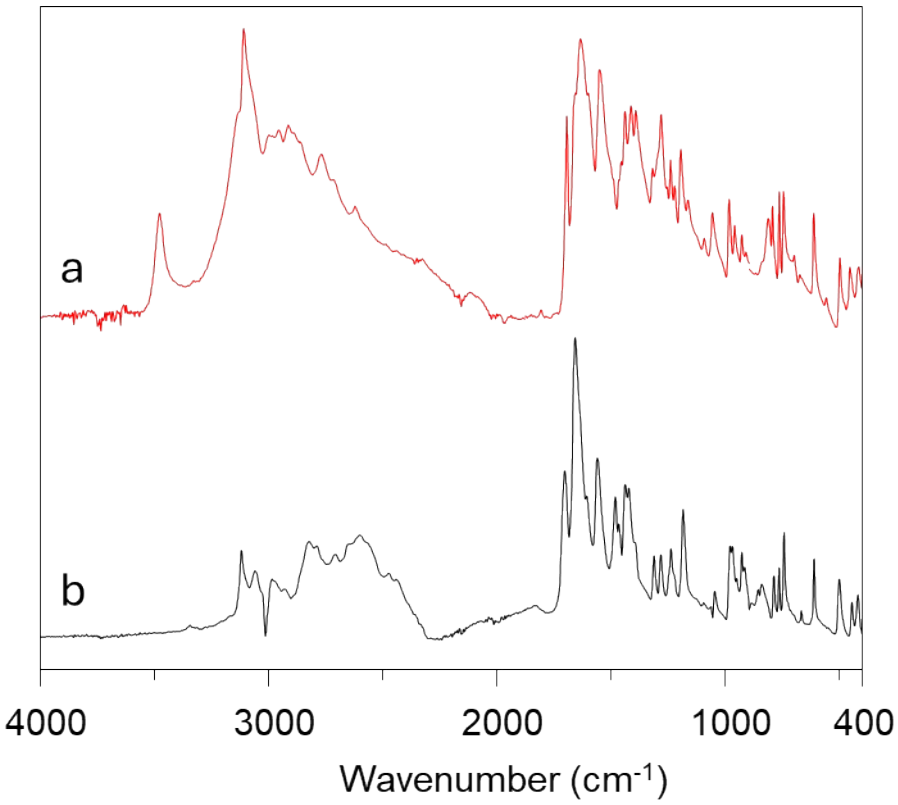

Fig. S1. FTIR spectra of theophylline peroxosolvate $C_7H_8N_4O_2 \bullet H_2O_2$ **1** (a) and theophylline (b).

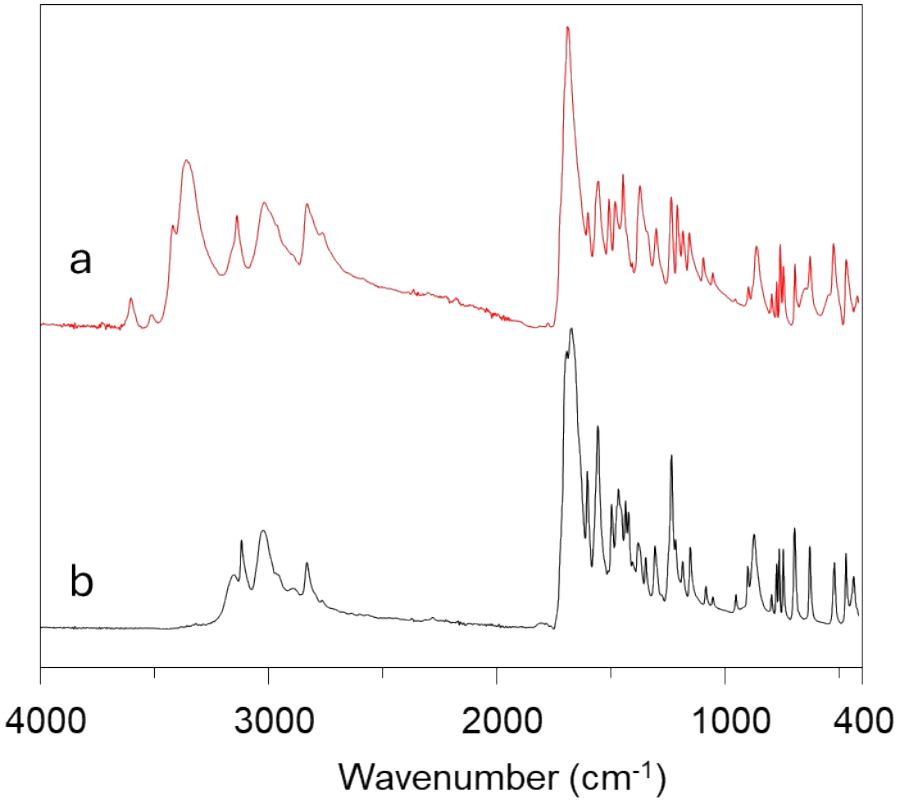

Fig. S2. FTIR spectra of theobromine peroxosolvate $C_7H_8N_4O_2 \bullet H_2O_2$ **2** (a) and theobromine (b).

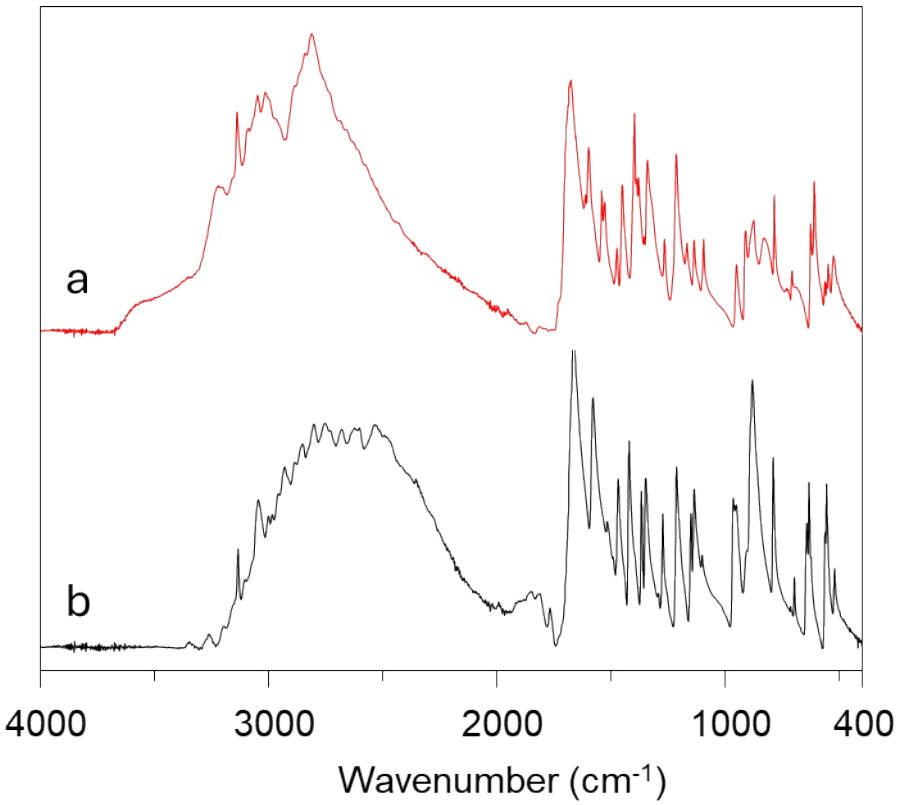

Fig. S3. FTIR spectra of hypoxanthine peroxosolvates **3**, **4** (a) and hypoxanthine (b).

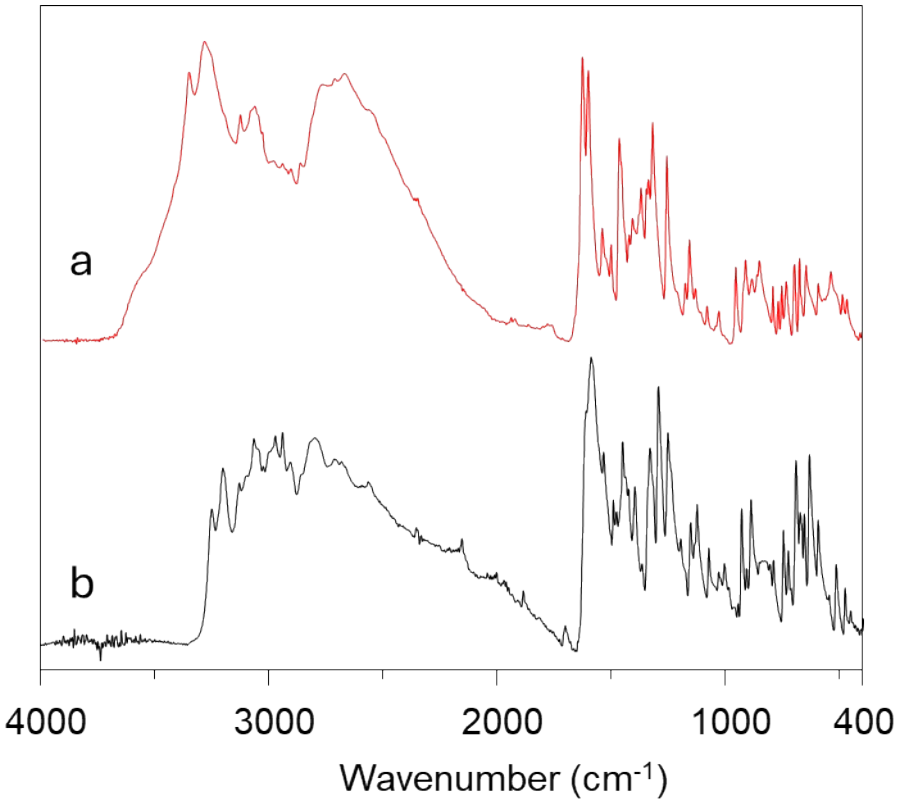

Fig. S4. FTIR spectra of benzylaminopurine peroxosolvates **5** (a) and benzylaminopurine (b).

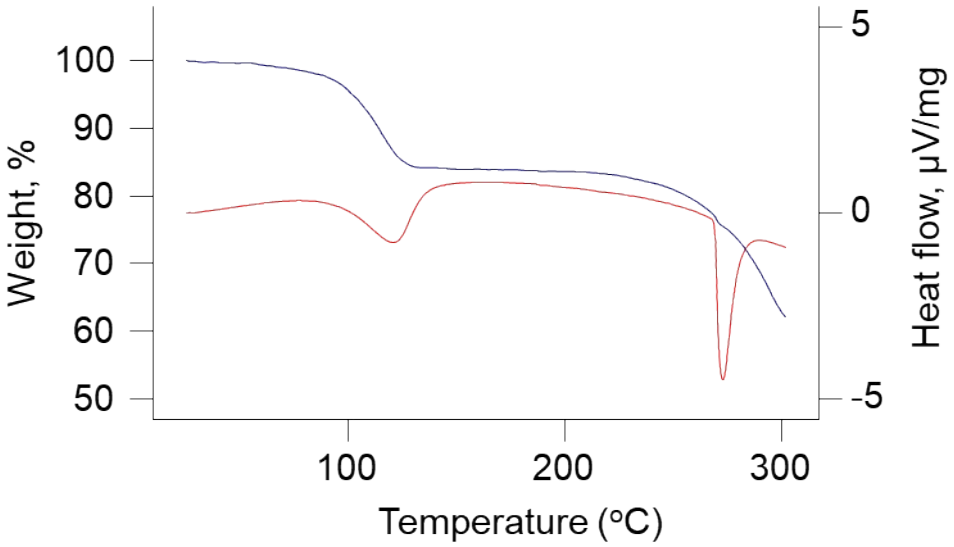

Fig. S5. TG (blue) and DTA (red) curves of theophylline peroxosolvate $C_7H_8N_4O_2 \bullet H_2O_2$ **1**.

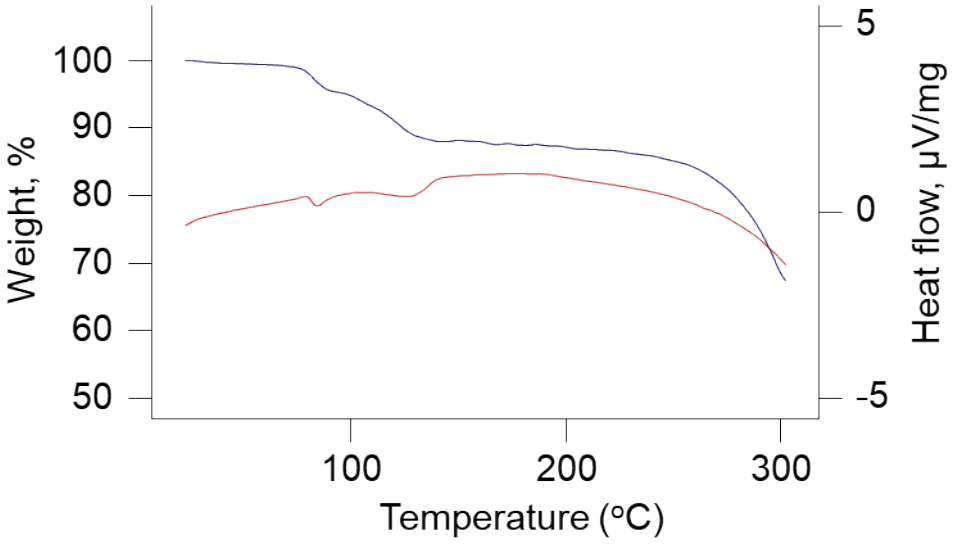

Fig. S6. TG (blue) and DTA (red) curves of theobromine peroxosolvate $C_7H_8N_4O_2 \bullet H_2O_2$ **2**.

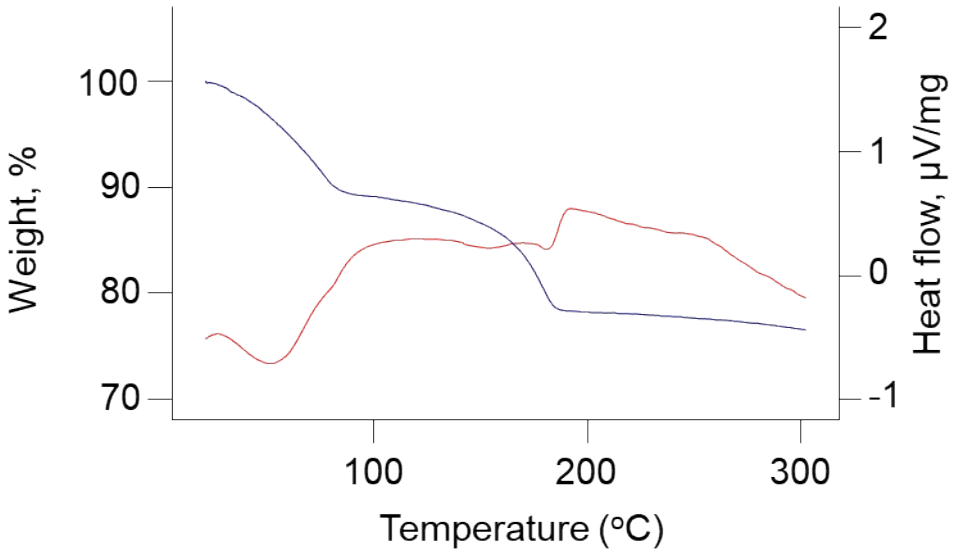

Fig. S7. TG (blue) and DTA (red) curves of of hypoxanthine peroxosolvates **3**, **4**.

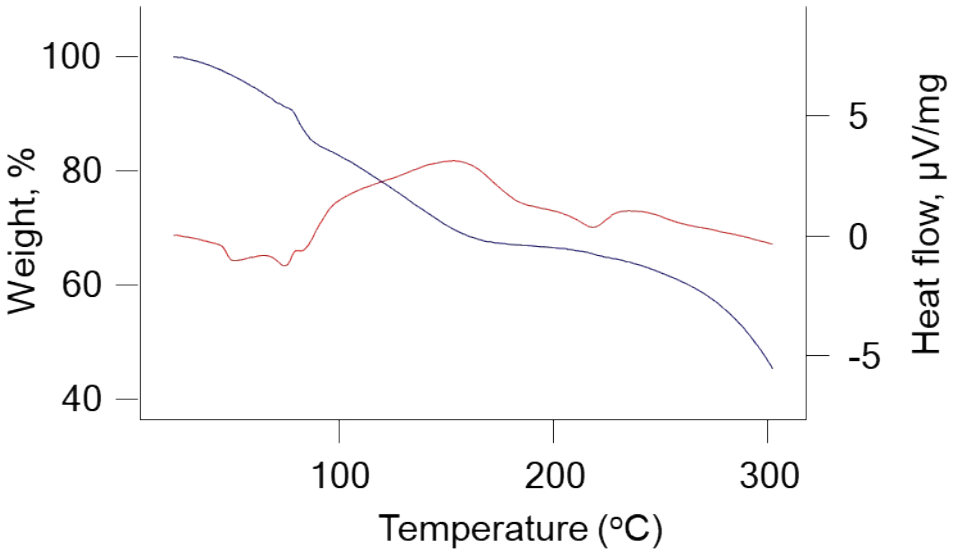

Fig. S8. TG (blue) and DTA (red) curves of benzylaminopurine peroxosolvate **5**.

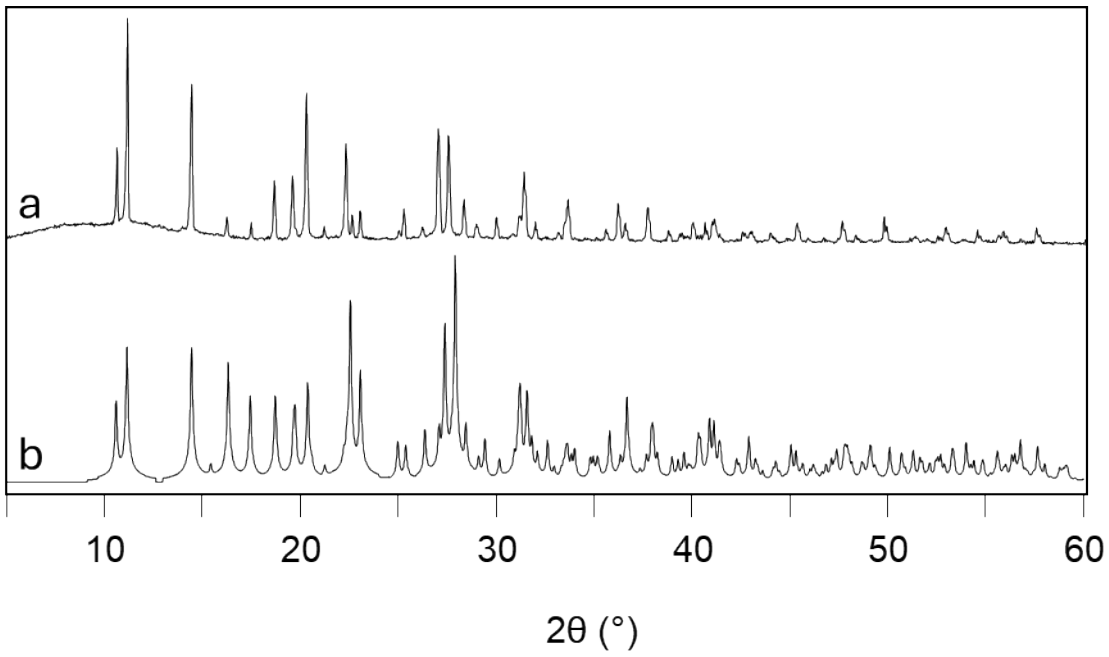

Fig. S9. Powder (a) and calculated X-Ray diffractogram (b) of theophylline peroxosolvate $C_7H_8N_4O_2 \bullet H_2O_2$ **1**.

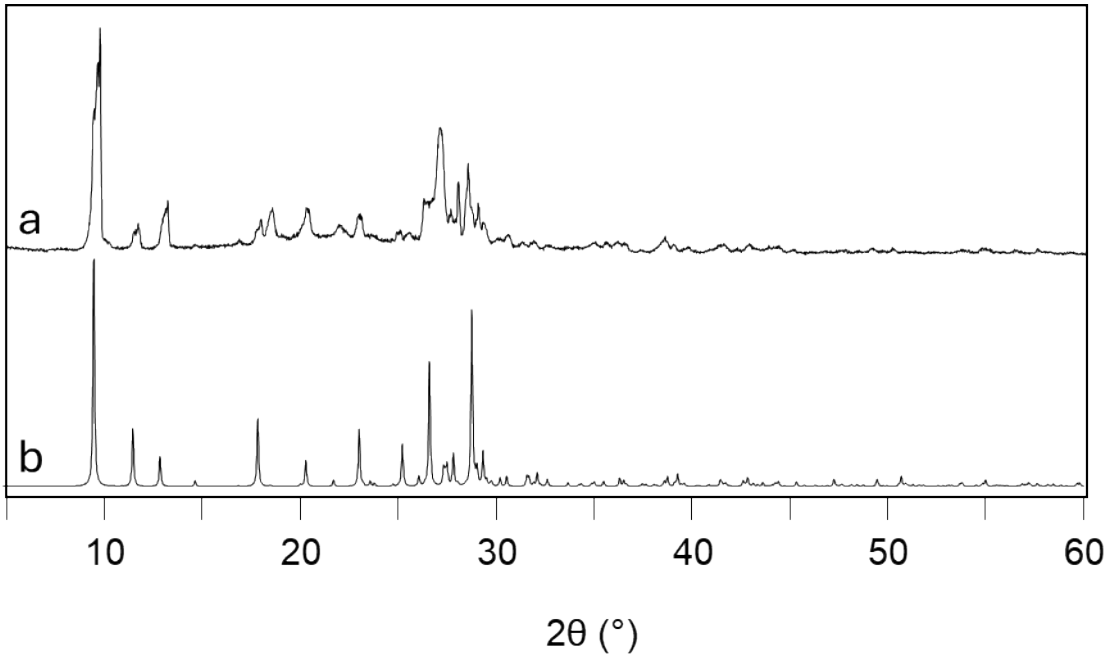

Fig. S10. Powder (a) and calculated X-Ray diffractogram (b) of theobromine peroxosolvate $C_7H_8N_4O_2 \bullet H_2O_2$ **2**.

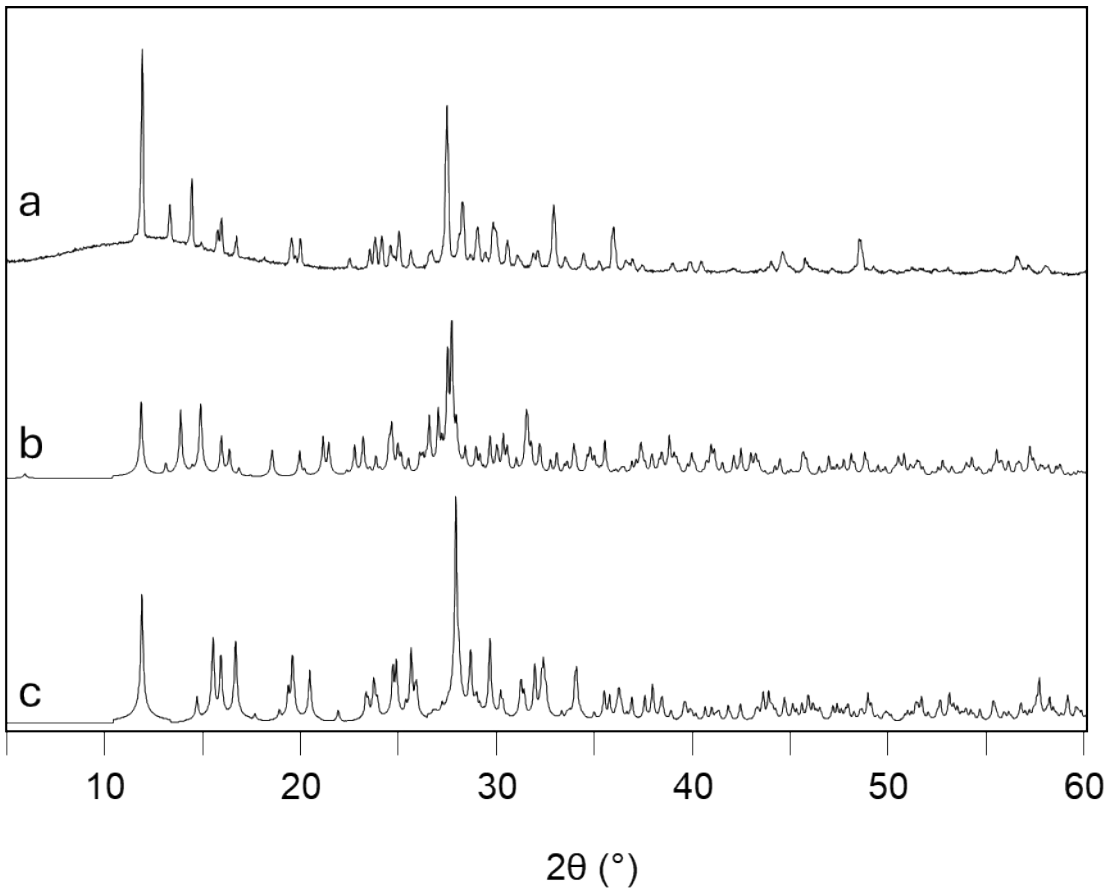

Fig. S11. Powder (a) and calculated X-Ray diffractogram (b, c) of hypoxanthine peroxosolvates **3** and **4**, respectively.

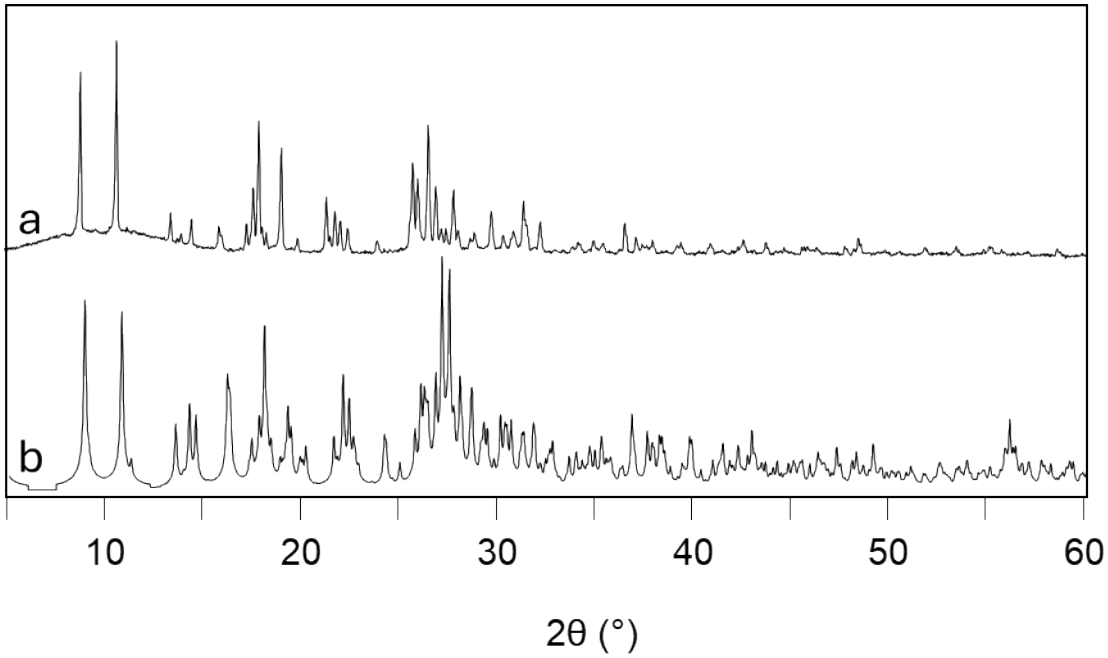

Fig. S12. Powder (a) and calculated X-Ray diffractogram (b) of benzylaminopurine peroxosolvate **5**.

Table S2. The difference between the calculated (B3LYP/6-31G**) and experimental values of the D···A distances. The energies E_{HB} (kJ·mol^{-1}) of H-bonds, evaluated using Equation S1.

1		
D–H…A	Δ(D…A), Å	E_{HB}, kJ·mol^{-1}
O1–H1…O2[a]	-0.014	22.9
O2–H2…N1	-0.019	32.6
N2–H20…O3	-0.035	34.7
C1–H10…O4	-0.075	20.7
3		
N11–H11…O21	-0.015	35.0
N21–H21…O11	-0.027	34.4
N14–H14…N12	0.005	22.2
N24–H24…N22	0	21.6
O1–H1…N23	-0.005	29.7
O2–H2…N13[C]	-0.013	28.7
C12–H12…O11	0	20.1
C24–H23…O1	-0.020	12.2
C22–H22…O21	-0.011	19.3

[a] See Figs. 1a,b; [b] See Figs. 3a,b.

Table S3. The experimental and calculated (B3LYP/6-31G**) values of the D···A distances and computed values of the electron density, ρ_b, the local electronic kinetic energy density, G_b at the hydrogen bonds critical point in theophylline peroxosolvate **1**. The energies E_{HB} (kJ·mol^{-1}) of H-bonds, evaluated using Equation S1.

D–H…A	*d*(D…A), Å				
	exp	calcd	ρ_b, a.u.	G_b a.u.	E_{HB}, kJ·mol^{-1}
O1–H1…O2[a]	2.842(1)	2.828	0.02618	0.02036	22.9
O2–H2…N1	2.766(1)	2.747	0.04591	0.02896	32.6
N2–H20…O3	2.782(1)	2.747	0.03921	0.03082	34.7
C1–H10…O4	3.052(1)	2.977	0.02246	0.01837	20.7

[a] See Figs. 1, 2 and 15.

Table S4. The experimental and calculated (B3LYP/6-31G**) values of the D···A distances and computed values of the electron density, ρ_b, the local electronic kinetic energy density, G_b at the hydrogen bonds critical point in theophylline peroxosolvate **3**. The energies E_{HB} (kJ·mol^{-1}) of H-bonds, evaluated using Equation S1.

D–H…A	*d*(D…A), Å				
	exp	calcd	ρ_b, a.u.	G_b a.u.	E_{HB}, kJ·mol^{-1}
N11–H11…O21	2.782(2)	2.767	0.04212	0.03106	35.0
N21–H21…O11	2.798(2)	2.771	0.04161	0.03056	34.4
N14–H14…N12	2.938(2)	2.943	0.03222	0.01970	22.2
N24–H24…N22	2.954(2)	2.954	0.03133	0.01913	21.6
O1–H1…N23	2.781(2)	2.776	0.04074	0.02640	29.7
O2–H2…N13[C]	2.814(2)	2.801	0.03971	0.02549	28.7
C12–H12…O11	3.065(2)	3.065	0.02401	0.01787	20.1
C24–H23…O1	3.184(3)	3.275	0.01452	0.01080	12.2
C22–H22…O21	3.081(2)	3.070	0.02289	0.01710	19.3

[a] See Figs. 1, 2 and 15.

Table S5. The experimental and calculated (B3LYP/6-31G**) values of the D···A distances and computed values of the electron density, ρ_b, the local electronic kinetic energy density, G_b at the hydrogen bonds critical point in theophylline hydrate.[11] The energies E_{HB} (kJ·mol^{-1}) of H-bonds, evaluated using Equation S1.

D–H…A	*d*(D…A), Å				
	exp	calcd	ρ_b, a.u.	G_b a.u.	E_{HB}, kJ·mol^{-1}
O1–H…N1[a]	2.898(5)	2.911	0.03029	0.01928	21.7
O1–H…O2	2.726(2)	2.683	0.04687	0.03502	39.4
O2–H…N6	2.882(5)	2.877	0.03192	0.02057	23.2
O2–H…O1	2.741(3)	2.718	0.04189	0.02057	35.0
C1–H…O1	3.193(4)	3.171	0.01764	0.01404	15.8
N2–H…O4	2.743(3)	2.757	0.03843	0.02994	33.7
N5–H…O2	2.758(4)	2.749	0.03968	0.03101	34.9

[a] See Fig. 15.

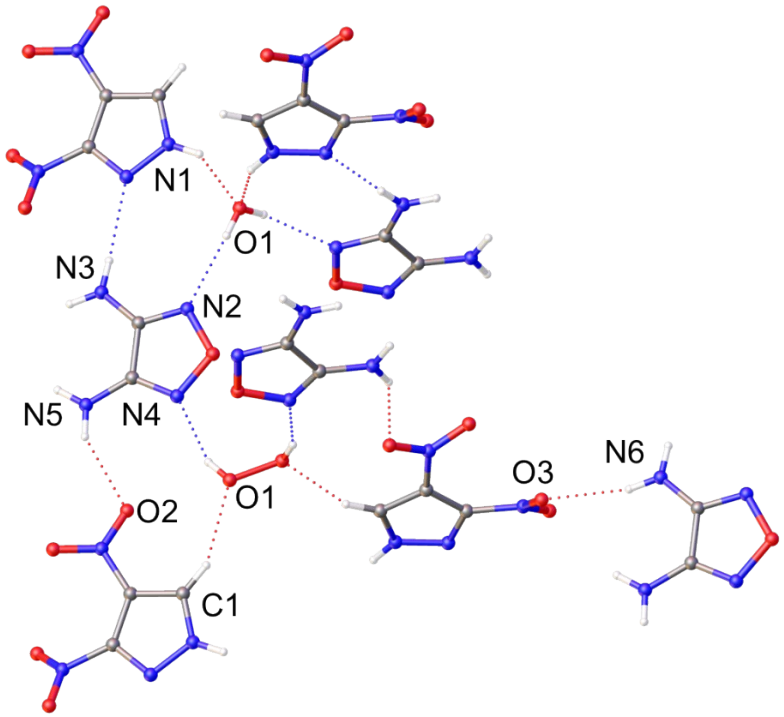

Fig. S13. Fragment of the crystal structure of DDD2 (refcode ZETPAT).[12] Hydrogen bonds are drawn by dashed lines.

Table S6. The experimental and calculated (B3LYP/6-31G**) values of the D···A distances and computed values of the electron density, ρ_b, the local electronic kinetic energy density, G_b at the hydrogen bonds critical point in DDD2 (refcode ZETPAT).[12] The energies E_{HB} (kJ·mol^{-1}) of H-bonds, evaluated using Equation S1.

D–H…A	*d*(D…A), Å				
	exp	calcd	ρ_b, a.u.	G_b a.u.	E_{HB}, kJ·mol^{-1}
N1–H…O1[a]	2.806(3)	2.775	0.03792	0.02688	30.3
O1–H…N2	2.894(3)	2.886	0.03108	0.02000	22.5
N3–H…N1	3.124(30	3.119	0.02044	0.01381	15.6
O1–H…N4	2.882(3)	2.878	0.0308	0.02034	22.9
C1–H…O1	3.134(3)	3.162	0.01633	0.01198	13.5
N5–H…O2	3.014(3)	2.994	0.01915	0.01379	15.5
N6–H…O3	3.133(3)	3.175	0.00843	0.00706	8.0

[a] See Fig. S13.

References

1. Mikhaylov, A. A. *et al.* Laboratory Method for Obtaining Anhydrous Hydrogen Peroxide and Safety Rules for Handling It. *Russ J Gen Chem* **94**, 3333–3339 (2024).
2. Schumb, W. C., Satterfield, C. N. & Wentworth, R. L. *Hydrogen Peroxide*. (Reinhold Publishing Corporation, New York, 1955). doi:10.1002/jps.3030450224.
3. Maass, O. & Hatcher, W. H. The properties of pure hydrogen peroxide. I. *J Am Chem Soc* **42**, 2539 (1920).
4. *APEX 3*. (2016).
5. Krause, L., Herbst-Irmer, R., Sheldrick, G. M. & Stalke, D. Comparison of silver and molybdenum microfocus X-ray sources for single-crystal structure determination. *J Appl Crystallogr* **48**, 3–10 (2015).
6. Sheldrick, G. M. Crystal structure refinement with SHELXL. *Acta Crystallogr C Struct Chem* **71**, 3–8 (2015).
7. Pedersen, B. F. The crystal structure of ammonium oxalate monoperhydrate. *Acta Crystallogr B* **28**, 746–754 (1972).
8. Pedersen, B. F. The observed shortening of the oxygen–oxygen bond in the hydrogen peroxide molecule in solids. *Acta Crystallogr B* **28**, 1014–1016 (1972).
9. Laus, G., Kahlenberg, V., Wurst, K., Lörting, T. & Schottenberger, H. Hydrogen bonding in the perhydrate and hydrates of 1,4-diazabicyclo[2.2.2]octane (DABCO). *CrystEngComm* **10**, 1638 (2008).
10. Churakov, A. V., Prikhodchenko, P. V. & Howard, J. A. K. The preparation and crystal structures of novel perhydrates Ph4X+Hal–·nH2O2: anionic hydrogen-bonded chains containing hydrogen peroxide. *CrystEngComm* **7**, 664 (2005).
11. Konovalova, I. S., Shishkina, S. V., Wyshusek, M., Patzer, M. & Reiss, G. J. Supramolecular architecture of theophylline polymorphs, monohydrate and co-crystals with iodine: study from the energetic viewpoint. *RSC Adv* **14**, 29774–29788 (2024).
12. Tariq, Q.-N. *et al.* Synthesis, Performance, and Thermal Behavior of Two Insensitive 3,4-Dinitropyrazole-Based Energetic Cocrystals. *Cryst Growth Des* **23**, 112–119 (2023).
13. Erba, A. *et al.* CRYSTAL23: A Program for Computational Solid State Physics and Chemistry. *J Chem Theory Comput* **19**, 6891–6932 (2023).
14. Cossard, A., Desmarais, J. K., Casassa, S., Gatti, C. & Erba, A. Charge Density Analysis of Actinide Compounds from the Quantum Theory of Atoms in Molecules and Crystals. *J Phys Chem Lett* **12**, 1862–1868 (2021).
15. Mata, I., Alkorta, I., Espinosa, E. & Molins, E. Relationships between interaction energy, intermolecular distance and electron density properties in hydrogen bonded complexes under external electric fields. *Chem Phys Lett* **507**, 185–189 (2011).
16. Bader, R. F. W. A quantum theory of molecular structure and its applications. *Chem Rev* **91**, 893–928 (1991).
17. Medvedev, A. G. *et al.* Fast Quantum Approach for Evaluating the Energy of Non-Covalent Interactions in Molecular Crystals: The Case Study of Intermolecular H-Bonds in Crystalline Peroxosolvates. *Molecules* **27**, 4082 (2022).